Proceedings of
ASME Turbo Expo 2002
June 3-6, 2002, Amsterdam, The Netherlands

GT-2002-30394

INVESTIGATIONS OF THE FLOW THROUGH A HIGH PRESSURE RATIO CENTRIFUGAL IMPELLER

Gernot Eisenlohr, formerly Rolls-Royce Deutschland Ltd&CoKG;

Hartmut Krain, DLR-Köln;
Franz-Arno Richter, MAN Turbomaschinen AG, GHH BORSIG;
Valentin Tiede, Kompressorenbau Bannewitz GmbH

ABSTRACT

In an industrial research project of German and Swiss Turbo Compressor manufacturers a high pressure ratio centrifugal impeller was designed and investigated. Performance measurements and extensive laser measurements (L2F) of the flow field upstream, along the blade passage and downstream of the impeller have been carried out. In addition to that, 3D calculations have been performed, mainly for the design point. Results have been presented by Krain et al., 1995 and 1998, Eisenlohr et al., 1998 and Hah et al.,1999.

During the design period of this impeller a radial blade at the inlet region was mandatory to avoid a rub at the shroud due to stress reasons. The measurements and the 3D calculations performed later, however, showed a flow separation at the hub near the leading edge due to too high incidence. Additionally a rather large exit width and a high shroud curvature near the exit caused a flow separation near the exit, which is enlarged by the radially transported wake of the already addressed hub separation.

Changes to the hub blade angle distribution to reduce the hub incidence and an adaptation of the shroud blade angle distribution for the same impeller mass-flow at the design point were investigated by means of 3D calculations first with the same contours at hub and shroud; this was followed by calculations with a major change of the shroud contour including an exit width change with a minor variation of the hub contour. These calculations showed encouraging results; some of them will be presented in conjunction with the geometry data of the original impeller design.

NOMENCLATURE

List of Symbols

Ma	Mach number [-]
LE	Blade leading edge
PS	pressure side
R	radius [m]
SS	suction side
SRV2-O	original blade design
SRV2-N	new blade, same contours
SRV5	new blade, new contours, small exit width design
T	temperature [K]
TE	Blade trailing edge
c	absolute velocity [m/s]
h	channel height hub to shroud
m	distance along shroud or hub
m	mass flow rate [kg/s]
n	shaft speed [rpm]
n_0	design speed [rpm]
p	pressure [N/m^2]
t	pitch
u	circumferential speed [m/s]
w	relative velocity [m/s]
x	kart. coordinate
y	kart. coordinate
z	kart. coordinate
z	distance from hub
α	absolute flow angle from tangential[deg]
β	relative flow angle from tangential[deg]
η	efficiency
ρ	density [kg /m^3]
π	pressure ratio [-]
ω	angular velocity [1/s]

Subscripts

1	rotor inlet
2	rotor exit
4	station at possible diffuser exit
ax	axial direction
is	isentropic
red	corrected (mass flow)
t	total
i	blade angle – flow angle
r_4/r_2	= 1.89

INTRODUCTION

As a consequence of the trend in centrifugal compressor designs to significantly reduce both size and weight for cost reasons without efficiency penalties the aerodynamic loading of the blades is increasing. This results in high Mach number designs with transonic inlet flow conditions. In the early nineties transonic flow phenomena in centrifugal compressors were not very well understood. In order to investigate these transonic flow phenomena, a centrifugal compressor with high specific speed, high pressure ratio and high mass flow coefficient was designed and built at DLR. The impeller (SRV2-O) design data are shown in **Table 1**.

inlet total pressure	p_{t1} =	101325	[N/m2]
inlet total temperature	T_{t1} =	288,15	[K]
shaft speed	n =	50000	[rpm]
specific speed	N_s =	105	Def. Balje
design mass flow rate	m =	2,55	[kg/s]
blade count full/splitter	z_f/z_s =	13/13	[-]
Leading **E**dge hub radius	r_{1h} =	30	[mm]
LE tip radius	r_{1t} =	78	[mm]
blade angle LE tip	$ß_{1t}$ =	26,5	[deg]
rel. Ma number tip inlet	Ma_{rel1t} =	1,3	[-]
impeller tip radius	r_2 =	112	[mm]
Exit blade height	b_{2ax} =	10,2	[mm]
Blade angle TE	$ß_2$ =	52	[deg]
impeller tip speed	u_2 =	586	[m/s]
impeller press. ratio	π_{12} =	6,1	[-]
efficiency	η_{t12} =	0,84	[-]

Table 1 : Impeller design data

Investigations of the performance map with conventional measurement techniques followed. The test rig and the measurement procedures used are described in detail by Krain and Hoffmann (1998).
Figure 1a shows the measured performance map of the stage with a vaneless diffuser.

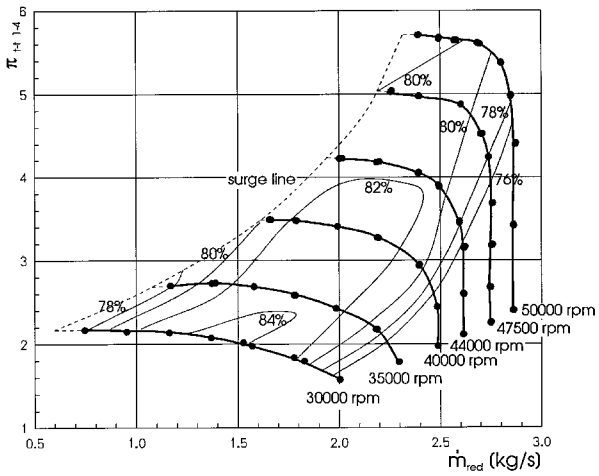

Figure 1: Performance Map SRV2-O with vaneless Diffuser

Here, the vaneless diffuser is a constant area diffuser, that mainly decelerates the circumferential velocity. The maximum stage pressure ratio at design speed is p_{t4}/p_{t1} = 5.7:1 with a corresponding isentropic efficiency η_{is4} of about 80%. An impeller performance map was derived from the measurements of total temperature, mass flow and static shroud pressure at impeller exit using continuity and Euler equation assuming 17% blockage; this value was taken from Krain et al., 1995. In **Figure 1b** the 100% speedline is plotted together with some calculated results which will be referred to later.

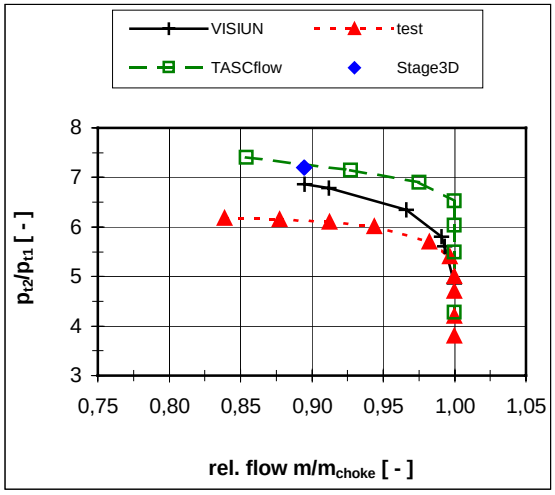

Figure 1b: Impeller Pressure ratio - SRV2-O at 100% speedline

Measurements of the flow-field were carried out with the L2F velocimetry technique developed by Schodl, 1989. The flow field at design conditions was also investigated with various numerical methods (Krain, Hoffmann, and Pak, 1995; Krain and Hoffmann, 1998; Eisenlohr et al., 1998 and Hah and Krain, 1999). This paper will first deal with some of the investigations carried out for the original impeller and it gives information about changes being made, some in actual hardware, most of them however theoretically to study the changes in the flow field within the rotating system in order to improve the diffuser inlet conditions. The purpose of this was and still is to improve the performance of the stage with a vaned diffuser. All measurement data referred to in this paper result from impeller configurations with the original blade design of SRV2-O; the geometry of this impeller will be given in an appendix.

ORIGINAL IMPELLER BLADE DESIGN

The impeller blade was designed applying loading distributions along hub and shroud traces. A linear connection between points of both traces generated a ruled surface which made it possible to manufacture the blades by flank milling. In an actual series production the impeller cusps left by the milling lines would not be removed; at this impeller, however, they had to be removed, as the L2F-velocimetry technique developed by Schodl, 1989 required a hub contour without residual milling lines. **Figure 2a** shows a front-view of hub and shroud traces of a full blade with some of the generating lines added. In **Figure 2b** the blade angle distributions along hub ($ß_s$-O,hub) and shroud ($ß_s$-O,shroud) are plotted versus the dimensionless meridional trace length m* = [m(i)-m(0)]/[m(TE)-m(0)]; m(0) is the meridional LE-position of SRV2-O at both traces.
The complete blade geometries together with hub and shroud contours of this original impeller are given in an **Appendix**. Near the leading

edge the full blade had to be radially oriented due to stress reasons. Therefore a high incidence occurred at design mass flow in the hub region. This can be seen in **Figure 3**; there the blade metal angle β_S at the leading edge (LE) of the main blade is plotted versus blade span. Relative flow angles β resulting from laser measurements and two NS flow solutions for the design mass flow are added. As already indicated by Eisenlohr et al.,1998 the incidence is far too high in the hub region. The associated spanwise axial velocity distribution at the inlet of this impeller is shown in **Figure 4**. Both, measurements and the calculations, showed a similar radial gradient in this distribution, which, however, was not expected to be that high.

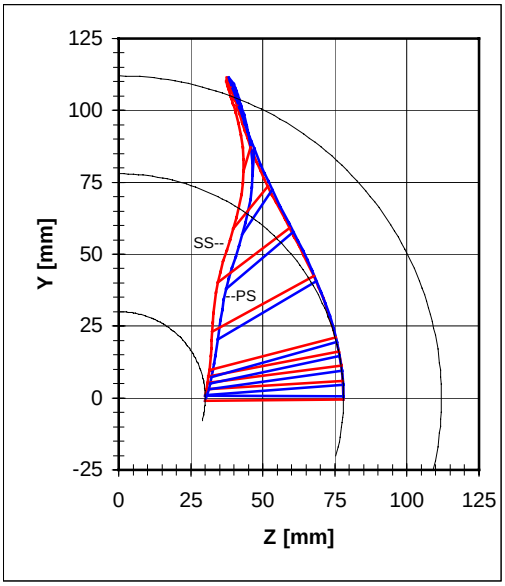

Figure 2a: Front view of impeller blade

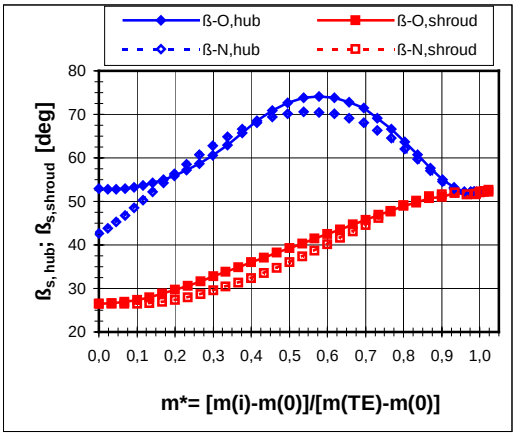

Figure 2b: Blade angle distribution along traces SRV2-O and SRV2-N

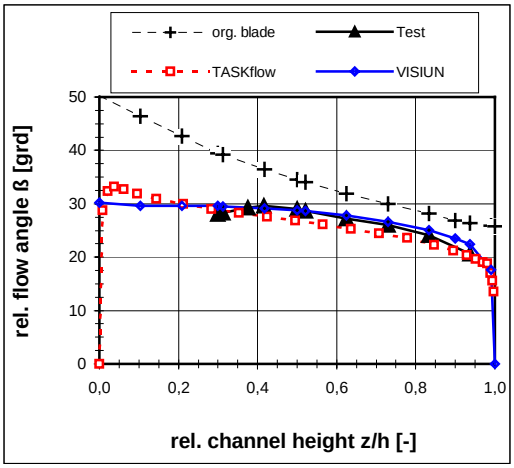

Figure 3: Radial distribution of flow angle beta: Original blade SRV2-O

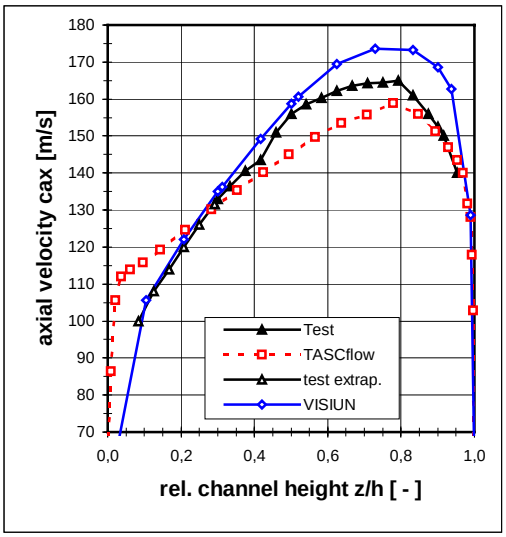

Figure 4 : Radial distribution of axial velocity Original blade SRV2-O

The distribution of the relative Mach number Ma_w at the exit of this impeller is shown in Figure 5. **Figure 5a** represents the measured distribution and **Figure 5b** the calculated distribution with FLOWSIM, Hoffmann, W.,1990, whereas **Figure 5c** shows the calculated distribution with VISIUN, revision 4.0, NREC, 1995. The measurement and FLOWSIM cuts are normal to the shroud contour, so that the hub region is met on a somewhat lower radius; with VISIUN a cylindrical cut just inside the blade exit is used. Even though the cuts through the exit are not absolutely the same, all the distributions, however, indicate that problems with a too strongly varying incidence could be expected with a downstream vaned diffuser preventing a good pressure recovery; these problems were actually experienced with a vaned diffuser and a modified contour design, before doing the theoretical investigations that are described here.

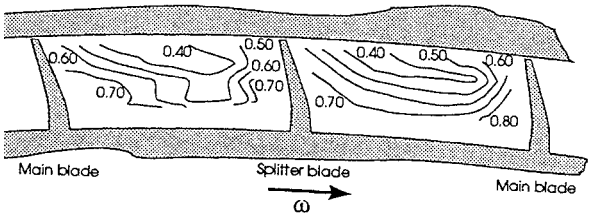

Figure 5a : Measured exit Mach number distribution Ma-w SRV2-O

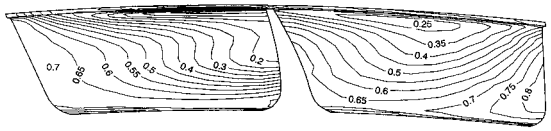

Figure 5b : Calculated exit Mach number distribution FLOWSIM: Ma-w SRV2-O

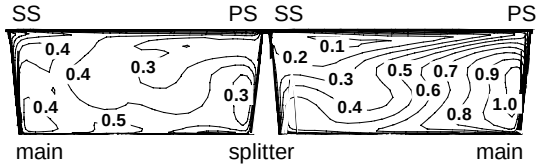

Figure 5c : Calculated exit Mach number distribution VISIUN: Ma-w SRV2-O

IMPELLER PRESSURE RATIO

For the design speed the characteristics for the impeller have been evaluated in more detail and are plotted in **Figures 6** versus relative mass flow m/m_{choke}. First the measured (test) characteristics and second the characteristics calculated for the original impeller (SRV2-O) should be compared. It should be mentioned that all the calculated characteristics referred here in Figures 6 a-c were evaluated with VISIUN, however the other programs used showed similar results for impeller pressure ratio, as can be seen in **Figure 1b**. As the pressure ratios differ significantly (**Figure 6a**) and the resulting efficiencies showed to be about the same level (**Figure 6c**), the work inputs to the fluid are obviously higher for the calculations than for the measurements (**Figure 6b**). Therefore it seems that neither the high deceleration of relative velocity along the shroud with the separation at TE, nor the flow separation at the hub leading edge seem to have influenced the work input to the flow in the calculation. Perhaps the turbulence models cannot solve this problem satisfactorily. However, no reasonable explanation for this result in the calculations was found.

NEW IMPELLER BLADE DESIGN

To eliminate the flow separation at the leading edge hub a new blade geometry has been created. This was done by closing the hub inlet angle by about 10 degrees; the new inlet angle distribution required that the hub trace had to be altered completely in order to limit the wrap angle change of the blade. As already mentioned by Eisenlohr et. al. 1998, the leading edge had to be swept axially backwards in order to maintain the design mass flow of the impeller.

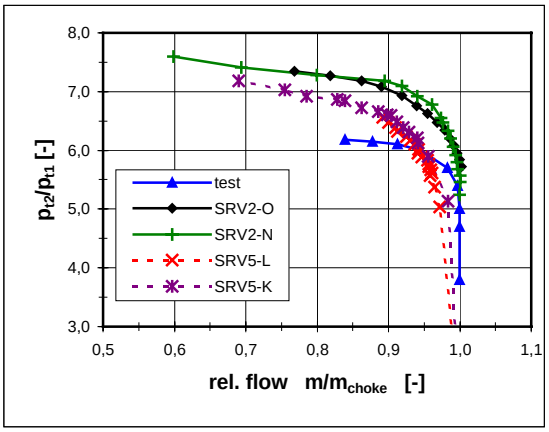

Figure 6a : Impeller total pressure ratio p_{t2}/p_{t1}

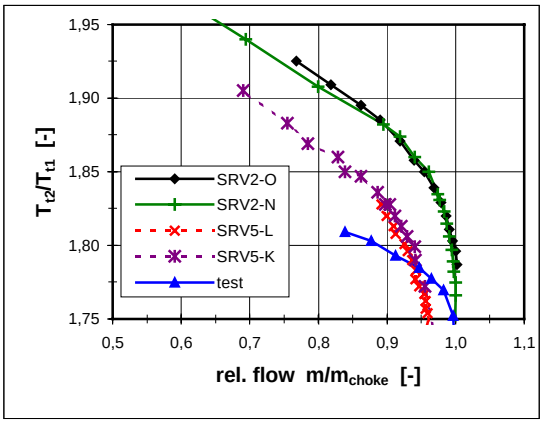

Figure 6b : Impeller total temperature ratio T_{t2}/T_{t1}

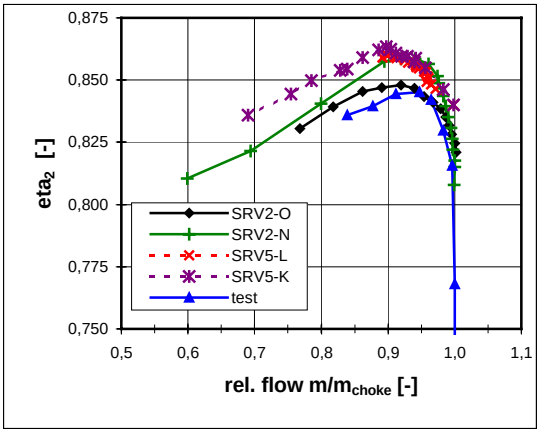

Figure 6c : Impeller isentropic efficiency η_{21}

Together with this, a slight change in the shroud angle distribution was necessary. The blade angle distributions ß$_s$ along hub and shroud trace of the new blade design are shown in **Figure 2b**. The shroud leading edge is located at m* = 0.067. To get better physical stress distributions at the blade roots a rake angle at the exit diameter was additionally introduced with about 2.4 degrees difference in wrap angle between hub and shroud, but having the same blade exit angle as the original design.

With this new blade (SRV2-N) the design speed characteristics were evaluated using the same hub and shroud contours as with SRV2-O; again VISIUN program was used, see **Figure 6**. The result proved the same mass flow at choke conditions. A little higher efficiency between choke and design mass flow resulted in a little higher pressure ratio in this field. Work input was just about the same.

At design mass flow again the distribution of the relative Mach number Ma_w at the exit of this new configuration was evaluated. **Figure 7a** shows the result calculated with the VISIUN program. This is quite a change in the distribution, but less than anticipated. **Figure 7b** shows the result for the same configuration obtained with FINE Turbo, revision 4.1; it looks somewhat smoother but confirming in principle the results obtained with the VISIUN program.

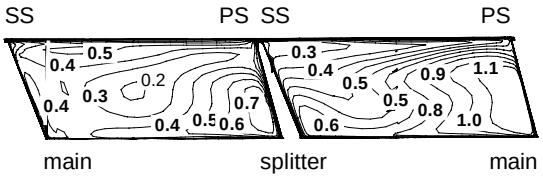

Figure 7a : Calculated exit Mach number distribution
VISIUN: Ma-w SRV2-N: Original exit width

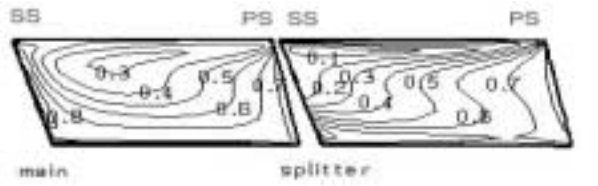

Figure 7b : Calculated exit Mach number distribution
Fine Turbo: Ma-w SRV2-N: Original exit width

MERIDIONAL CONTOUR CHANGES

As the shroud separation for the tested SRV2-O impeller was not solely due to the separation caused by the high hub incidence, but also due to the high deceleration within the impeller resulting from a large exit width, an axial contour shift reducing the exit width for about 15% was theoretically investigated. For this configuration the relative Mach number Ma_w at the exit was evaluated; the result is shown in **Figure 8**. The mean value of the velocities seem to have just risen a bit but the distribution as such is quite similar; however the reverse flow to the impeller at the shroud was supressed.

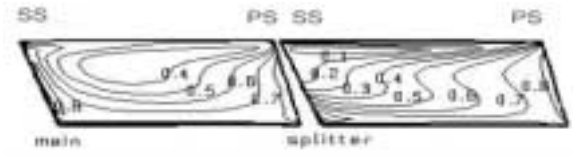

Figure 8 : Calculated exit Mach number distribution
Fine Turbo: Ma-w SRV2-N : Smaller exit width

In hardware a vaned diffuser had been introduced with the hub contour downstream of the original impeller (SRV2-O) following the impeller exit slope of 13 degrees from radial. The vane height was constant and adapted to the original impeller exit width. The performance map of this configuration is shown in **Figure 9a**. The efficiency η_{t-t} is lower than with the vaneless constant area diffuser configuration. It is obvious that the problems expected in chapter 'Original Impeller design' are predominant. The high deceleration near the shroud caused a separation bubble with reverse flow to the impeller; also it was not possible to use the L2F method in parts of the vaneless diffuser region because of too high turbulence.

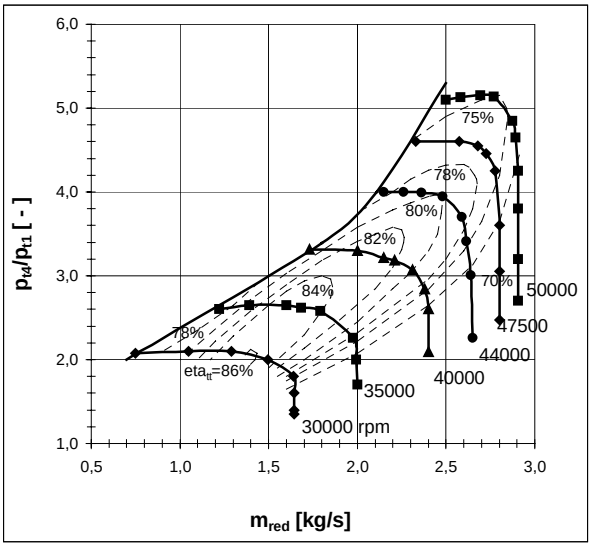

Figure 9a : Performance map SRV2-O : Original impeller exit width with vaned diffuser

The original impeller was investigated with a conical vaneless diffuser also, first using the old impeller exit width and then with the reduced exit width. There the total pressure characteristic improved and also did the static pressure rise; this proved the strong separation along the shroud contour due to too high deceleration together with the hub incidence problem mentioned before. Otherwise the pressure characteristic should have resulted in a lower pressure ratio due to the change of reaction by squeezing the impeller exit. With the squeezing the reverse flow to the impeller could be supressed and the vanes then could cope better with the varying incidence.

As done in the calculations for the new blade design the impeller exit width together with the diffuser vane height was reduced by the same axial contour shift as mentioned before; the performance map was again determined, which is shown in **Figure 9b**. The pressure ratio

$Pi_{tot} = \pi_{tot} = p_{t4}/p_{t1}$ recovered to the values with vaneless diffuser measured between the same stations. As the efficiency is higher at low speeds a slightly more squeezed impeller exit could even raise the pressure ratio, however loosing range at low speeds.

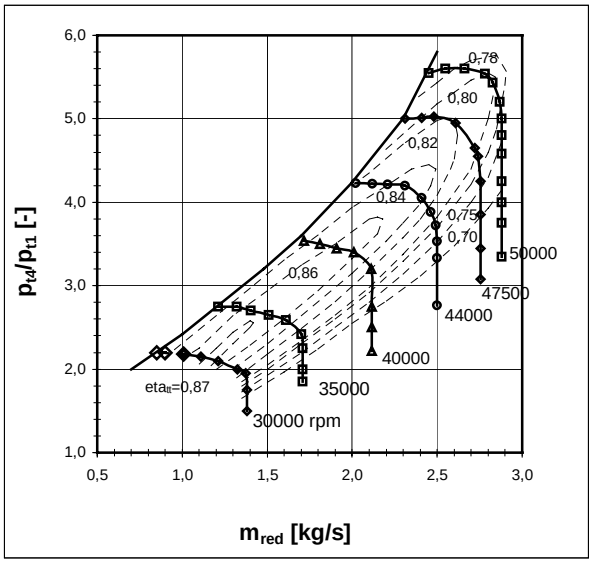

Figure 9b : Performance map SRV2-O : Reduced impeller exit width with vaned diffuser

As the curvature at the shroud contour is increasing in direction to the impeller exit at the original design a complete change of the contour design was also theoretically investigated with following alteration: The hub contour downstream of the impeller should follow the impeller exit slope of 13 degrees from radial. To improve shroud curvature distribution maximum curvature was moved upstream to establish a decreasing curvature towards the impeller exit, approaching zero curvature at a parallel cone to the hub contour at about 1.135 radius ratio just ahead of the intended LE for a vaned diffuser. The result of the calculation for the relative Mach number Ma_w distribution at impeller exit with these new contours (SRV5) is shown in **Figure 10**. The distribution is distinctly smoother but still not as homogeneous as was expected.

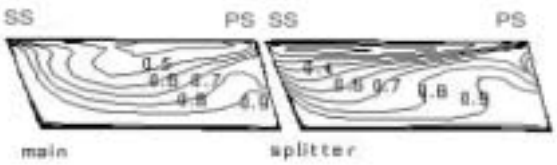

Figure 10 : Calculated exit Mach number distribution Fine Turbo: Ma-w SRV5 : Modified shroud contour

The characteristics resulting from calculations with this new contour were also added in **Figure 6** together with the results of the previous calculations. The differences in the addendum –L and -K to SRV5 are two different tries for the extension of the calculation grid after the trailing edge of the impeller. There was no influence seen at impeller exit. The impeller efficiency is higher, however pressure ratio and temperature ratio are lower than with the calculations of the original design. This is surely due to the change of deceleration in the impeller, but still it is not as low as with the measurements of the original design.

Also the incidence along the LE span with the new blade (SRV2-N) was investigated, this time using TASCflow and Fine Turbo. **Figure 11** shows the new blade angle distribution together with the flow angle distribution. The incidence now seems to be acceptable.

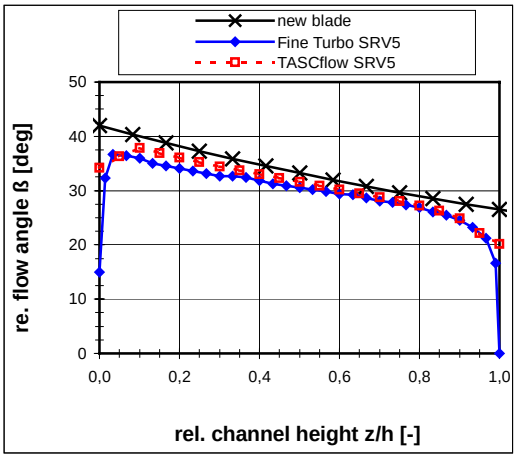

Figure 11: Radial distribution of flow angle beta: New blade SRV5 contours

The associated spanwise axial velocity distribution at the inlet is shown in **Figure 12.** The gradient is reduced but still high.

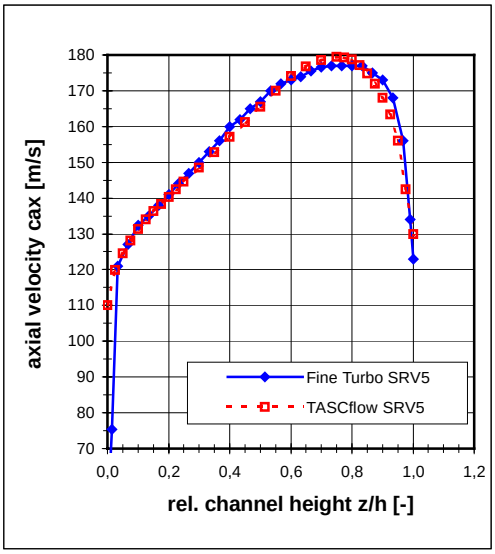

Figure 12 : Radial distribution of axial velocity: New blade SRV5 contours

CONCLUSIONS

The investigations presented here showed that the interaction of blade design and meridional contours is much more sensitive for high pressure ratio impellers with high transonic relative inlet velocities than for those impellers having only subsonic inlet conditions. Keeping the main dimensions (r_{1h}; r_{1t}; r_2; $ß_{2Blade}$; l_{ax}) of the high specific speed impeller unchanged in the 'numerical experiment' as well as in the measurements, means were examined to improve unfavourable flow conditions.

At the impeller exit the flow separation due to too high deceleration could be reduced by squeezing the exit width by about 15%. This was proved with the original impeller blade design (SRV2-O) by CFD-calculations and performance measurements. The flow separation at hub leading edge due to high incidence was fully eliminated by a new blade design (SRV2-N) when leaving the stress requirements of a radial blade (no blade lean) design at LE region for SRV2-O and proved by the CFD-calculations.

The exit velocity gradient mainly resulting from shroud curvature could not be reduced by the amount envisaged. The new blade design together with the contour changes was investigated theoretically. An additional reduction of radial flow area in the vaneless diffuser to limit the ability of boundary layer separation onset together with a longer impeller having less shroud curvature should be investigated in detail before going again into hardware.

ACKNOWLEDGEMENTS

The project has been sponsored by the German Ministry of Economy via AIF and FVV (AIF = Arbeitsgemeinschaft Industrieller Forschungsvereinigungen , BMWi/AIF-Nr. : 9849/12033 and FVV = Forschungsvereinigung Verbrennungskraftmaschinen e.V, FVV-Nr. : 604/67290). The authors wish to thank these Organizations and the participating companies for permission to publish parts of the results.

REFERENCES

Eisenlohr, G.; Dalbert, P.; Krain, H.; Pröll, H.; Richter, F.A. and Rohne, K.H.: Analysis of the Transonic Flow at the Inlet of a High Pressure Ratio Centrifugal Impeller", ASME 98-GT-24, 1998.

FINE/Turbo, Manual: NUMECA's Flow Integrated Environment for Turbomachinery and Internal Flows; User manual Version 4.1, Brussels, April 2000

Hah, C; Krain,H. : Analysis of the Transonic Flow Fields inside a High Pressure Ratio Centrifugal Compressor at Design and Off Design Conditions, ASME 99-GT-446, 1999.

Hirsch, Ch.; Kang, S.; Pointel, G.: "A numerically supported investigation of the 3D flow in centrifugal impellers", ASME 96-GT-152, 1996

Hoffmann,W.: „A Computer Program System for the Analysis of 3D Steady Flows in Turbomachinery„, (in German).DLR-FB90-18, 1990.

Krain, H.; Hoffmann, B. and Pak, H. : „ Aerodynamics of a Centrifugal Compressor Impeller with Transonic Inlet Conditions", ASME 95-GT-79, 1995.

Krain, H. Hoffmann, B.: „ Flow Physics in High Pressure Ratio Centrifugal Compressors", ASME FEDSM98-4853, 1998.

NREC: Northern Research and Engineering Corporation: „Simultanious Three-Dimensional CFD-Analysis of Rotating and Stationary Bladed Passages in Turbomachinery, A Computational System„, Massachusetts, 1995.

Schodl, R. 1989, „Measurement Techniques in Aerodynamics", VKI Lecture Series 1989.

APPENDIX :

The information of the APPENDIX can be found on following Web-Site : http://www.dlr.de/SRV2

Impeller blade coordinates and meridional contours:

The generating lines of the main blade and the splitter blade are put down in the following tables:

1. The pressure side main blade is described by **Table 2**, the suction side by **Table 3**.
2. The pressure side splitter blade is described by **Table 4**, the suction side splitter blade by **Table 5**.
3. Meridional Contours of **H**ub, **C**asing and impeller **S**hroud are listed in **Table 6**.

A right handed Cartesian Coordinate system is used, X being the axis of the impeller,
see **App. Fig. 1 and 2**.

The X = 0 coordinate being where the X- coordinate of hub contour is meeting the exit radius. Therefore all X-Coordinates do have negative values starting with the main blade inlet at the most negative values. The contours are shown in **App. Figure 2**.
Both, the main and splitter blade leading edges should be rounded with a 3:1 ellipse in flow direction. The ellipse will be tangent to a 90 deg. cone: Full blade at X = -75.0 mm ; Splitter at X= -51.5 mm.
Trailing edge at R = 112 mm.

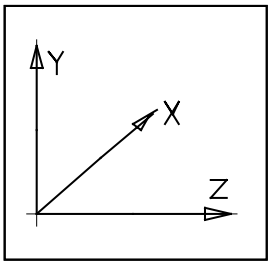

App. Fig. 1: Coordinate system

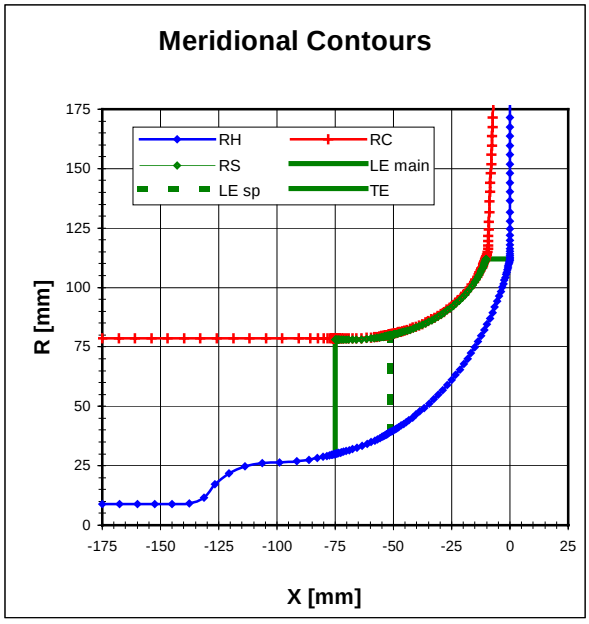

App. Fig. 2 : Meridional contours SRV2-O

Table 2: Pressure side main blade

LN	XS,P	YS,P	ZS,P	XH,P	YH,P	ZH,P
1	-75.0000	-0.6250	77.9975	-74.8065	-0.8981	30.0280
2	-72.3905	4.5002	77.8701	-72.1945	1.0250	30.6355
3	-69.7810	9.5803	77.4094	-69.5822	3.0290	31.2163
4	-67.1717	14.5671	76.6484	-66.9704	5.1243	31.7608
5	-64.5642	19.4097	75.6697	-64.3614	7.2942	32.2656
6	-61.9611	24.0771	74.5074	-61.7577	9.5316	32.7294
7	-59.3651	28.5463	73.1965	-59.0561	11.9168	33.1691
8	-56.7790	32.8110	71.7697	-56.1476	14.5534	33.6008
9	-54.2057	36.8718	70.2589	-53.0696	17.4110	34.0220
10	-51.6480	40.7391	68.6911	-49.8475	20.4741	34.4372
11	-49.1090	44.4276	67.0887	-46.4989	23.7329	34.8636
12	-46.5920	47.9558	65.4696	-43.0757	27.1405	35.3244
13	-44.1007	51.3436	63.8469	-39.6030	30.6730	35.8586
14	-41.6388	54.6096	62.2323	-36.1424	34.2739	36.5073
15	-39.2103	57.7676	60.6377	-32.7343	37.9106	37.3062
16	-36.8199	60.8333	59.0730	-29.3895	41.6062	38.2713
17	-34.4720	63.8244	57.5425	-26.1940	45.3133	39.3616
18	-32.1723	66.7558	56.0508	-23.1280	49.1049	40.5445
19	-29.9264	69.6409	54.6027	-20.2499	52.9447	41.7510
20	-27.7408	72.4925	53.2012	-17.5603	56.8635	42.9286
21	-25.6226	75.3218	51.8496	-15.1034	60.7986	44.0034
22	-23.5796	78.1390	50.5503	-12.8022	64.8852	44.9559
23	-21.6201	80.9545	49.3041	-10.7561	68.9329	45.6971
24	-19.7536	83.7775	48.1102	-8.8452	73.1659	46.2240
25	-17.9900	86.6162	46.9678	-7.1511	77.3857	46.4724
26	-16.3403	89.4789	45.8719	-5.6059	81.7207	46.4234
27	-14.8181	92.3695	44.8151	-4.2435	86.0301	46.0627
28	-13.4320	95.3005	43.7836	-2.9919	90.4948	45.3694
29	-12.1974	98.2727	42.7638	-1.9356	94.7240	44.4328
30	-11.1262	101.2878	41.7396	-1.0774	98.5409	43.4139
31	-10.5000	103.3522	41.0363	-0.5946	100.8571	42.7381
32	-10.2300	104.3449	40.6958	-0.3808	101.9305	42.4129
33	-9.9521	105.3978	40.3289	-0.1629	103.0537	42.0645
34	-9.6683	106.4817	39.9435	0.0513	104.1825	41.7065
35	-9.3532	107.6814	39.5070	0.2842	105.4277	41.3032
36	-9.0279	108.9113	39.0489	0.5182	106.6786	40.8876
37	-8.7027	110.1381	38.5810	0.7530	107.9263	40.4631
38	-8.3779	111.3613	38.1045	0.9878	109.1709	40.0295

Table 3: Suction side main blade

LN	XS,S	YS,S	ZS,S	XH,S	YH,S	ZH,S
1	-75.0000	0.6250	77.9975	-75.2035	0.8851	29.9440
2	-72.3905	5.9445	77.7731	-72.5949	3.0557	30.3994
3	-69.7810	11.1777	77.1949	-69.9854	5.2818	30.7972
4	-67.1717	16.2531	76.3087	-67.3751	7.5328	31.1415
5	-64.5642	21.1505	75.2017	-64.7667	9.8103	31.4367
6	-61.9611	25.8436	73.9132	-62.1623	12.1112	31.6899
7	-59.3651	30.3173	72.4809	-59.4587	14.5310	31.9127
8	-56.7790	34.5676	70.9403	-56.5472	17.1736	32.1172
9	-54.2057	38.6017	69.3236	-53.4643	20.0197	32.3036
10	-51.6480	42.4316	67.6587	-50.2347	23.0540	32.4827
11	-49.1090	46.0758	65.9677	-46.8749	26.2685	32.6782
12	-46.5920	49.5545	64.2680	-43.4359	29.6218	32.9214
13	-44.1007	52.8844	62.5766	-39.9414	33.0946	33.2583
14	-41.6388	56.0838	60.9070	-36.4531	36.6295	33.7451
15	-39.2103	59.1732	59.2668	-33.0134	40.2028	34.4161
16	-36.8199	62.1700	57.6646	-29.6364	43.8390	35.2827
17	-34.4720	65.0886	56.1084	-26.4111	47.4920	36.2977
18	-32.1723	67.9429	54.6058	-23.3187	51.2269	37.4275
19	-29.9264	70.7480	53.1605	-20.4184	55.0047	38.6007
20	-27.7408	73.5171	51.7762	-17.7113	58.8491	39.7658
21	-25.6226	76.2634	50.4544	-15.2413	62.7003	40.8428
22	-23.5796	78.9986	49.1961	-12.9321	66.6857	41.8107
23	-21.6201	81.7342	48.0003	-10.8815	70.6245	42.5734
24	-19.7536	84.4790	46.8675	-8.9700	74.7334	43.1237
25	-17.9900	87.2426	45.7938	-7.2771	78.8237	43.3948
26	-16.3403	90.0339	44.7727	-5.7341	83.0168	43.3737
27	-14.8181	92.8557	43.7987	-4.3729	87.1778	43.0528
28	-13.4320	95.7213	42.8557	-3.1217	91.4835	42.4114
29	-12.1974	98.6335	41.9248	-2.0616	95.5692	41.5321
30	-11.1262	101.5955	40.9851	-1.1959	99.2721	40.5672
31	-10.5000	103.6278	40.3353	-0.7070	101.5267	39.9253
32	-10.2300	104.6062	40.0193	-0.4902	102.5725	39.6165
33	-9.9521	105.6441	39.6794	-0.2696	103.6672	39.2861
34	-9.6683	106.7124	39.3231	-0.0532	104.7683	38.9465
35	-9.3532	107.8948	38.9204	0.1808	105.9834	38.5640
36	-9.0279	109.1069	38.4989	0.4147	107.2045	38.1697
37	-8.7027	110.3162	38.0688	0.6490	108.4228	37.7666
38	-8.3779	111.5221	37.6313	0.8836	109.6384	37.3552

Table 4: Pressure side splitter

LN	XS,P	YS,P	ZS,P	XH,P	YH,P	ZH,S
1	-56.7790	33.6357	71.3869	-56.1707	15.5860	33.1218
2	-54.2057	37.4263	69.9652	-53.0894	18.0563	33.6717
3	-51.6480	40.9845	68.5450	-49.8609	20.8158	34.2224
4	-49.1090	44.5422	67.0127	-46.5060	23.8933	34.7481
5	-46.5920	48.0186	65.4235	-43.0797	27.1992	35.2757
6	-44.1007	51.3723	63.8238	-39.6047	30.6883	35.8438
7	-41.6388	54.6203	62.2229	-36.1428	34.2739	36.5068
8	-39.2103	57.7691	60.6363	-32.7343	37.9105	37.3063
9	-36.8199	60.8327	59.0737	-29.3895	41.6062	38.2713
10	-34.4720	63.8243	57.5426	-26.1940	45.3133	39.3616
11	-32.1723	66.7557	56.0509	-23.1280	49.1049	40.5445
12	-29.9264	69.6409	54.6027	-20.2499	52.9447	41.7510
13	-27.7408	72.4925	53.2012	-17.5603	56.8635	42.9286
14	-25.6226	75.3218	51.8496	-15.1034	60.7986	44.0034
15	-23.5796	78.1390	50.5503	-12.8022	64.8852	44.9559
16	-21.6201	80.9545	49.3041	-10.7561	68.9329	45.6971
17	-19.7536	83.7775	48.1102	-8.8452	73.1659	46.2240
18	-17.9900	86.6162	46.9678	-7.1511	77.3857	46.4724
19	-16.3403	89.4789	45.8719	-5.6059	81.7207	46.4234
20	-14.8181	92.3695	44.8151	-4.2435	86.0301	46.0627
21	-13.4320	95.3005	43.7836	-2.9919	90.4948	45.3694
22	-12.1974	98.2727	42.7638	-1.9356	94.7240	44.4328
23	-11.1262	101.2878	41.7396	-1.0774	98.5409	43.4139
24	-10.5000	103.3522	41.0363	-0.5946	100.8571	42.7381
25	-10.2300	104.3449	40.6958	-0.3808	101.9305	42.4129
26	-9.9521	105.3978	40.3289	-0.1629	103.0537	42.0645
27	-9.6683	106.4817	39.9435	0.0513	104.1825	41.7065
28	-9.3532	107.6814	39.5070	0.2842	105.4277	41.3032
29	-9.0279	108.9113	39.0489	0.5182	106.6786	40.8876
30	-8.7027	110.1381	38.5810	0.7530	107.9263	40.4631
31	-8.3779	111.3613	38.1045	0.9878	109.1709	40.0295

Table 5: Suction side splitter

LN	XS,S	YS,S	ZS,S	XH,S	YH,S	ZH,P
1	-56.7790	33.7480	71.3339	-56.5656	16.1264	32.6456
2	-54.2057	38.0523	69.6267	-53.4797	19.3630	32.6917
3	-51.6480	42.1895	67.8100	-50.2457	22.7037	32.7205
4	-49.1090	45.9630	66.0463	-46.8812	26.1034	32.8049
5	-46.5920	49.4927	64.3155	-43.4394	29.5594	32.9741
6	-44.1007	52.8563	62.6004	-39.9429	33.0774	33.2738
7	-41.6388	56.0734	60.9166	-36.4535	36.6288	33.7454
8	-39.2103	59.1718	59.2683	-33.0134	40.2030	34.4160
9	-36.8199	62.1706	57.6639	-29.6364	43.8390	35.2827
10	-34.4720	65.0887	56.1084	-26.4111	47.4920	36.2977
11	-32.1723	67.9430	54.6057	-23.3187	51.2269	37.4275
12	-29.9264	70.7480	53.1605	-20.4184	55.0047	38.6007
13	-27.7408	73.5171	51.7762	-17.7113	58.8491	39.7658
14	-25.6226	76.2634	50.4544	-15.2413	62.7003	40.8428
15	-23.5796	78.9986	49.1961	-12.9321	66.6857	41.8107
16	-21.6201	81.7342	48.0003	-10.8815	70.6245	42.5734
17	-19.7536	84.4790	46.8675	-8.9700	74.7334	43.1237
18	-17.9900	87.2426	45.7938	-7.2771	78.8237	43.3948
19	-16.3403	90.0339	44.7727	-5.7341	83.0168	43.3737
20	-14.8181	92.8557	43.7987	-4.3729	87.1778	43.0528
21	-13.4320	95.7213	42.8557	-3.1217	91.4835	42.4114
22	-12.1974	98.6335	41.9248	-2.0616	95.5692	41.5321
23	-11.1262	101.5955	40.9851	-1.1959	99.2721	40.5672
24	-10.5000	103.6278	40.3353	-0.7070	101.5267	39.9253
25	-10.2300	104.6062	40.0193	-0.4902	102.5725	39.6165
26	-9.9521	105.6441	39.6794	-0.2696	103.6672	39.2861
27	-9.6683	106.7124	39.3231	-0.0532	104.7683	38.9465
28	-9.3532	107.8948	38.9204	0.1808	105.9834	38.5640
29	-9.0279	109.1069	38.4989	0.4147	107.2045	38.1697
30	-8.7027	110.3162	38.0688	0.6490	108.4228	37.7666
31	-8.3779	111.5221	37.6313	0.8836	109.6384	37.3552

Table 6: Meridional Contours

Impeller SRV2-O

Hub-Contour		**C**asing Contour		Imp.**S**hroud Contour	
Ax Coord	Radius	Ax Coord	Radius	Ax Coord	Radius
XH [mm]	RH [mm]	XC [mm]	RC [mm]	XS [mm]	RS [mm]
-175.000	9.000	-175.000	78.500	-75.000	78.000
-167.507	9.000	-167.973	78.500	-74.730	78.000
-160.015	9.000	-160.947	78.500	-74.410	78.000
-152.522	9.000	-153.920	78.500	-74.010	78.000
-145.029	9.002	-146.893	78.500	-73.540	78.000
-137.545	9.045	-139.867	78.500	-72.960	78.000
-131.403	11.626	-132.840	78.500	-72.270	78.000
-126.662	17.359	-125.813	78.500	-71.430	78.000
-120.604	21.738	-118.787	78.500	-70.410	78.000
-113.710	24.644	-111.760	78.500	-69.170	78.003
-106.367	26.078	-104.734	78.500	-67.680	78.015
-98.880	26.328	-97.707	78.500	-65.880	78.059
-91.409	26.872	-90.680	78.500	-63.700	78.119
-86.252	27.562	-85.801	78.500	-61.520	78.322
-82.694	28.194	-82.412	78.500	-59.720	78.500
-80.237	28.703	-80.059	78.500	-58.240	78.681
-78.538	29.092	-78.425	78.500	-57.020	78.849
-77.364	29.385	-77.290	78.500	-56.020	79.003
-76.550	29.594	-76.502	78.500	-55.180	79.140
-75.985	29.740	-75.954	78.500	-54.500	79.257
-75.593	29.842	-75.574	78.500	-53.930	79.357
-75.321	29.913	-75.310	78.500	-53.470	79.445
-75.132	29.962	-75.127	78.500	-53.080	79.526
-75.000	29.996	-75.000	78.500	-52.760	79.593
-74.720	30.059	-74.730	78.500	-52.500	79.643
-74.390	30.157	-74.410	78.500	-52.250	79.689
-73.980	30.248	-74.010	78.500	-51.980	79.746
-73.490	30.373	-73.540	78.500	-51.680	79.810
-72.890	30.524	-72.960	78.500	-51.340	79.882
-72.180	30.710	-72.270	78.500	-50.970	79.964
-71.310	30.942	-71.430	78.500	-50.560	80.057
-70.260	31.229	-70.410	78.500	-50.110	80.162
-69.000	31.594	-69.180	78.503	-49.600	80.282
-67.480	32.058	-67.680	78.515	-49.040	80.419
-65.650	32.656	-65.880	78.559	-48.420	80.578
-63.450	33.433	-63.700	78.619	-47.720	80.760
-61.280	34.272	-61.520	78.764	-46.950	80.971
-59.510	35.010	-59.730	78.940	-46.100	81.214
-58.050	35.655	-58.250	79.116	-45.140	81.498
-56.860	36.208	-57.020	79.282	-44.080	81.831
-55.880	36.680	-56.020	79.435	-42.900	82.221
-55.080	37.078	-55.190	79.568	-41.590	82.682
-54.420	37.416	-54.500	79.686	-40.270	83.180
-53.870	37.698	-53.930	79.788	-38.930	83.711
-53.430	37.936	-53.470	79.877	-37.600	84.277
-53.060	38.128	-53.080	79.945	-36.250	84.885
-52.750	38.299	-52.760	80.011	-34.910	85.532
-52.500	38.440	-52.500	80.055	-33.560	86.222
-52.090	38.663	-52.260	80.116	-32.210	86.955
-51.630	38.918	-51.990	80.171	-30.860	87.735
-51.130	39.201	-51.690	80.234	-29.520	88.560
-50.580	39.521	-51.360	80.306	-28.180	89.435
-49.960	39.879	-50.990	80.387	-26.850	90.363
-49.280	40.292	-50.580	80.478	-25.540	91.341
-48.520	40.757	-50.130	80.582	-24.240	92.371
-47.670	41.285	-49.620	80.701	-22.950	93.458
-46.740	41.887	-49.070	80.838	-21.700	94.601
-45.700	42.573	-48.450	80.994	-20.460	95.799
-44.550	43.359	-47.760	81.175	-19.260	97.054
-43.280	44.256	-46.990	81.383	-18.090	98.366
-41.870	45.284	-46.140	81.625	-16.970	99.734
-40.320	46.464	-45.200	81.907	-15.990	101.030
-38.620	47.816	-44.140	82.236	-15.140	102.240
-36.760	49.366	-42.970	82.623	-14.400	103.370
-34.730	51.146	-41.670	83.080	-13.760	104.420
-32.720	52.998	-40.360	83.573	-13.200	105.390
-30.750	54.923	-39.040	84.099	-12.720	106.290
-28.820	56.914	-37.710	84.661	-12.300	107.110
-26.920	58.968	-36.380	85.262	-11.930	107.870
-25.070	61.087	-35.050	85.902	-11.610	108.560
-23.270	63.257	-33.710	86.582	-11.330	109.200
-21.530	65.487	-32.380	87.307	-11.090	109.780
-19.840	67.757	-31.050	88.075	-10.870	110.310
-18.200	70.078	-29.720	88.888	-10.680	110.790
-16.640	72.429	-28.400	89.751	-10.510	111.230
-15.130	74.819	-27.090	90.664	-10.360	111.630
-13.690	77.229	-25.790	91.625	-10.230	112.000
-12.310	79.662	-24.510	92.637		
-11.010	82.103	-23.250	93.705		
-9.770	84.555	-22.000	94.827		
-8.600	86.996	-20.790	96.003		
-7.500	89.432	-19.590	97.235		
-6.470	91.850	-18.440	98.523		
-5.500	94.241	-17.320	99.867		
-4.680	96.390	-16.350	101.140		
-3.980	98.320	-15.500	102.330		
-3.380	100.050	-14.760	103.450		
-2.870	101.610	-14.110	104.480		
-2.420	103.010	-13.560	105.440		
-2.030	104.280	-13.070	106.330		
-1.700	105.420	-12.640	107.150		
-1.400	106.460	-12.270	107.900		
-1.150	107.400	-11.950	108.590		
-0.920	108.250	-11.660	109.220		
-0.720	109.030	-11.410	109.790		
-0.540	109.740	-11.190	110.320		
-0.380	110.380	-10.990	110.800		
-0.250	110.970	-10.820	111.240		
-0.130	111.510	-10.670	111.640		
-0.030	112.000	-10.530	112.000		
-0.020	112.580	-10.330	112.550		
-0.020	113.280	-10.090	113.210		
-0.010	114.130	-9.800	114.010		
0.000	115.150	-9.500	114.990		
0.000	116.390	-9.410	116.220		
0.000	117.890	-9.420	117.740		
0.000	119.710	-9.340	119.560		
0.000	121.900	-9.250	121.760		
0.000	124.560	-9.150	124.430		
0.000	127.780	-9.030	127.650		
0.000	131.670	-8.880	131.550		
0.000	136.380	-8.700	136.270		
0.000	140.280	-8.550	140.180		
0.000	144.170	-8.400	144.080		
0.000	148.060	-8.250	147.980		
0.000	151.950	-8.100	151.880		
0.000	155.850	-7.950	155.790		
0.000	159.740	-7.800	159.690		
0.000	163.630	-7.650	163.590		
0.000	167.520	-7.500	167.490		
0.000	171.420	-7.360	171.400		
0.000	175.310	-7.210	175.300		
0.000	179.200	-7.060	179.200		